Equivalent Material analysis of Triply Periodic Minimal Surfaces

Emilio Adrian Ramirez Salazar, Nicolas Béraud, Franck Pourroy, François Villeneuve, Matthieu Museau

Equivalent Material analysis of Triply Periodic Minimal Surfaces

E. A. Ramírez [a], N. Béraud [a], F. Pourroy [a], F. Villeneuve [a], M. Museau [a]

a. Univ. Grenoble Alpes, CNRS, Grenoble INP*, G-SCOP, 38000 Grenoble, France
* Institute of Engineering Univ. Grenoble Alpes
emilio-adrian.ramirez-salazar@grenoble-inp.fr

Résumé :

La fabrication de formes organiques complexes pour des produits mécaniques métalliques devient possible grâce aux progrès actuels des technologies de fabrication additive. En particulier, l'utilisation de surfaces minimales triples périodiques (TPMS), en tant qu'éléments de constructions cellulaires, a montré un potentiel pour la conception de structures légères, étant donné leurs avantages par rapport à la conception traditionnelle de treillis. Les motifs TPMS, qui sont des surfaces ouvertes définies mathématiquement avec une aire minimale locale, une courbure moyenne nulle et une périodicité tridimensionnelle, peuvent être utilisés pour créer des matériaux avec des renforcements continus et interconnectés grâce à leurs transitions douces entre les cellules unitaires. Dans cet article, la réponse mécanique des TPMS à base de coques d'épaisseur constante est explorée. À cette fin, des modèles Primitifs et Gyroïdes, qui sont des exemples courants de TPMS, de densités relatives diverses sont conçus en suivant une méthodologie de modélisation précédemment établie. L'analyse par éléments finis est utilisée pour tester la réponse mécanique de ces constructions sous des charges de compression et de cisaillement dans deux scénarios : une cellule unitaire unique et un assemblage matriciel de cellules. Les réponses des deux cas testés sont comparées et discutées. En conséquence, des modèles de loi de puissance des propriétés mécaniques en fonction de la densité relative des motifs sont proposés dans un contexte d'analyse par matériaux équivalents ou par métamatériaux. Les résultats de l'étude aideront potentiellement à la corrélation des résultats de l'analyse par éléments finis avec les méthodologies de conception des matériaux cellulaires à gradient fonctionnel de densité, dans le but de développer des structures optimisant simultanément la résistance et le poids.

Mots clés : Surface minimale triplement périodique, propriétés mécaniques, analyse par éléments finis, métamatériaux, fabrication additive

Abstract :

The manufacturing of complex organic shapes for metallic mechanical products is becoming possible due to current advances in additive manufacturing technologies. In particular, the use of Triply Periodic Minimal Surfaces (TPMS), as elements for cellular constructs, have shown potential for the design of lightweight structures, given their advantages over traditional lattices design. TPMS patterns, being mathematically-defined open surfaces with a local minimal area, zero mean curvature and three-

dimensional periodicity, can be used to create materials with continuous and interconnected reinforcements due to their smooth transitions between unit-cells. In this paper, the mechanical response of constant-thickness shell-based TPMS is explored. For this purpose, Primitive and Gyroid patterns, which are common examples of TPMS, of diverse relative densities are designed following a previously established modelling methodology. Finite Element Analysis is used to test the mechanical response of these constructs under compression and shear loads in two scenarios: a single pattern unit-cell and a matrix assembly of patterns. The response of the two tested cases are compared and discussed. As a result, power law models of mechanical properties as a function of the patterns' relative density are proposed under a framework of Equivalent Material or Metamaterial analysis. The outcomes of the study will potentially aid in the correlation of Finite Element Analysis results with design methodologies of Functionally Graded Cellular Materials with variable density, in an effort to develop structures with a simultaneous optimization of strength and weight.

Keywords : Triply Periodic Minimal Surface, Mechanical Properties, Finite Element Analysis, Metamaterials, Additive Manufacturing

1 Introduction

The development of highly complex structures is feasible due to the technological advancements of Additive Manufacturing (AM). To benefit from the freedoms offered by these fabrication processes, Design for Additive Manufacturing (DFAM) techniques have been developed to include cellular structure design, among other design methodologies [1]. Cellular materials, which are low-density structures capable of producing a simultaneous weight, stiffness and strength optimization [2], can be divided in stochastic (foams) or non-stochastic materials. In particular, non-stochastic or lattice materials characterized by an organized distribution of single unit-cells, provides a reliable control of deformation compared to foam structures [3].

Current studies on metamaterials, which are rationally designed materials with mechanical properties directly related to the topology of their micro-architecture [4], have focused on the implementation of Triply Periodic Minimal Surfaces (TPMS) due to their overall better mechanical performance compared to traditional lattices [5] and their capability of creating continuous and interconnected interfaces [6]. However, there is no predominant investigation on TPMS structures [7]. In general, TPMS are non-self-intersecting structures with a three-dimensional periodicity [8]. The fundamental shape of TPMS is defined to have a local zero-mean curvature [9] and described by a mathematical approximation from nodal equations [10]. To obtain a dense representation of the surface, two methods can be followed. The first method consists on closing one side of the minimal surface, thus obtaining a strut or solid-network-based structure [7]. The second method consists on using the TPMS as a central surface to be thickened, obtaining a sheet-based construct [11], [12]. It has been determined that strut-based constructs have problems of surface interconnectivity in low-density scenarios [13], while sheet-based structures present an overall better defined curvature [7].

Being cellular constructs, the mechanical properties of TPMS depends on the surface topology [14], and its characteristics are more significant than the used material [15]. For this, a common approach used in the literature is to refer the mechanical responses as dimensionless parameters under the Gibson-Ashby model [16]. Even though the response sheet-based TPMS constructs under compressive loads have been extensively studied in the literature [5], [6], [17]–[23], few studies have analysed this type of structures

under shear scenarios. Furthermore, there is no information for the determination of the Gibson-Ashby model's coefficients from Finite Element simulations of structures formed by an arrangement of patterns' unit-cell.

Therefore, the present study explores the mechanical response of sheet-based Primitive and Gyroid patterns, which are two of the most common TPMS examples, following a study of relative density dependency on the pattern thickness and unit-cell size [24]. Single pattern unit-cells and a structured assembly of pattern instances with different thickness are tested following an equivalent material analysis framework. Accordingly, an equivalent material is defined as a material with a dimension corresponding to the bounding box of the pattern assembly structure, filled with a dense material whose mechanical properties are similar to the properties of the pattern structure [25]. Both scenarios are tested under compressive and shear loads to establish dimensionless mechanical parameters as a function of the pattern's relative density.

The outcomes of this study are aimed towards the development of Functionally Graded Cellular Materials (FGCM) based on TPMS structures with variable density. Ultimately, the proposed equations for equivalent parameters in this paper can be used to relate the results of stress and deformation from Finite Element Analysis (FEA) to a mapped density distribution.

2 Methods

2.1 TPMS shape modelling

The generation of the fundamental shape of the TPMS is obtained as a zero level-set approximation from the surface's equation, following a previously established procedure for implicit surface modelling by scalar field polygonization [26]. The process, developed as a C# script under the Grasshopper environment of Rhinoceros 7 CAD suite, creates a scalar field from the evaluation of the mathematical definition for Primitive and Gyroid patterns, detailed on Eq. 1 and Eq. 2, respectively, at the positions of a predefined rectangular point-cloud representing the design space.

$$f_P(x,y,z) = \cos\left(\frac{2\pi x}{L}\right) + \cos\left(\frac{2\pi y}{L}\right) + \cos\left(\frac{2\pi z}{L}\right) \quad \text{Eq. 1}$$

$$f_G(x,y,z) = \cos\left(\frac{2\pi x}{L}\right)\sin\left(\frac{2\pi y}{L}\right) + \cos\left(\frac{2\pi y}{L}\right)\sin\left(\frac{2\pi z}{L}\right) + \cos\left(\frac{2\pi z}{L}\right)\sin\left(\frac{2\pi x}{L}\right) \quad \text{Eq. 2}$$

The field values are processed through a Marching Tetrahedra algorithm to develop the pattern's mesh, as illustrated on Fig. 1. This algorithm analyses the field in a discrete manner by grouping adjacent points representing a voxel, which are then subdivided as six tetrahedrons. The triangular facets of the mesh are formed depending if the tetrahedron corners are located above or below the TPMS surface, following 8 cases of scalar values distribution. As depicted by Fig. 1c, corners in opposite sides are represented by a change of circle's colour. When all corners are located in the same side, no facets are created. Additional details and the working principles of the algorithm are detailed on [27].

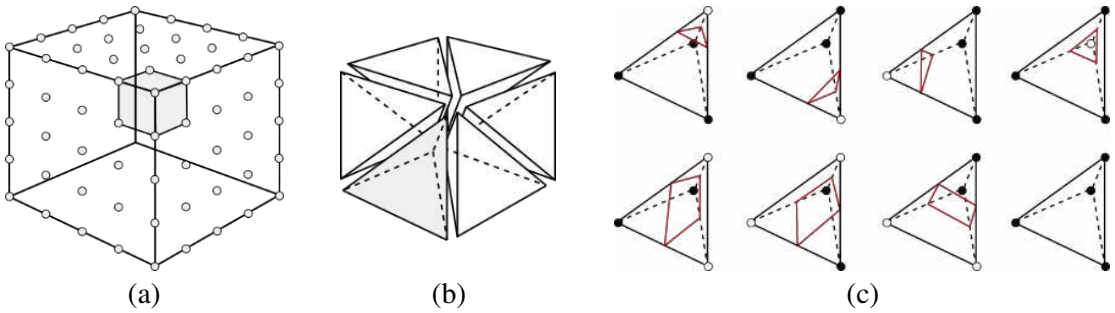

Fig. 1. Modelling by Marching Tetrahedra algorithm: a) Scalar field representation of the design space, b) voxel division in tetrahedrons and c) mesh facets creation from tetrahedra corner values.

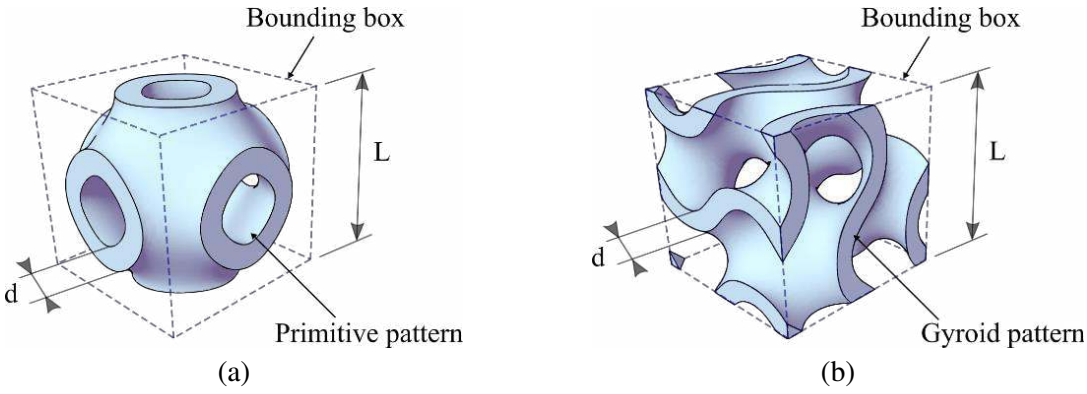

Fig. 2. Constant-thickness models for a) Primitive and b) Gyroid TPMS unit-cells.

As stated before, the solid representation of the patterns can be obtained by assigning a thickness d to the resulting shell surface. Accordingly, Fig. 2 shows examples for constant-thickness Primitive and Gyroid unit-cells. For the context of this study, the unit-cell size, represented by the length L, is set to a value of 50mm. Thickness values between 2 and 10mm are assigned in the FE modelling stages. These design specifications were selected due to previous manufacturing constraints considerations for the determination of the patterns' relative density function [24].

2.2 Finite Element modelling

Finite element analysis was conducted on shell models meshed by SHELL181 elements with constant thickness values by using Ansys® Academic Research Mechanical, Release 2020 R2. Two simulation scenarios under compression and shear loads are considered: a single pattern unit-cell and a matrix arrangement of patterns. For the single unit-cell scenario, models were simulated under periodic boundary conditions (PBC) for uniaxial loading and simple shear [28]. The applied PBCs are summarized below. Unconstrained coordinates are set as free. Traction boundary conditions are not considered, as their requirement is satisfied by the finite element process [29].

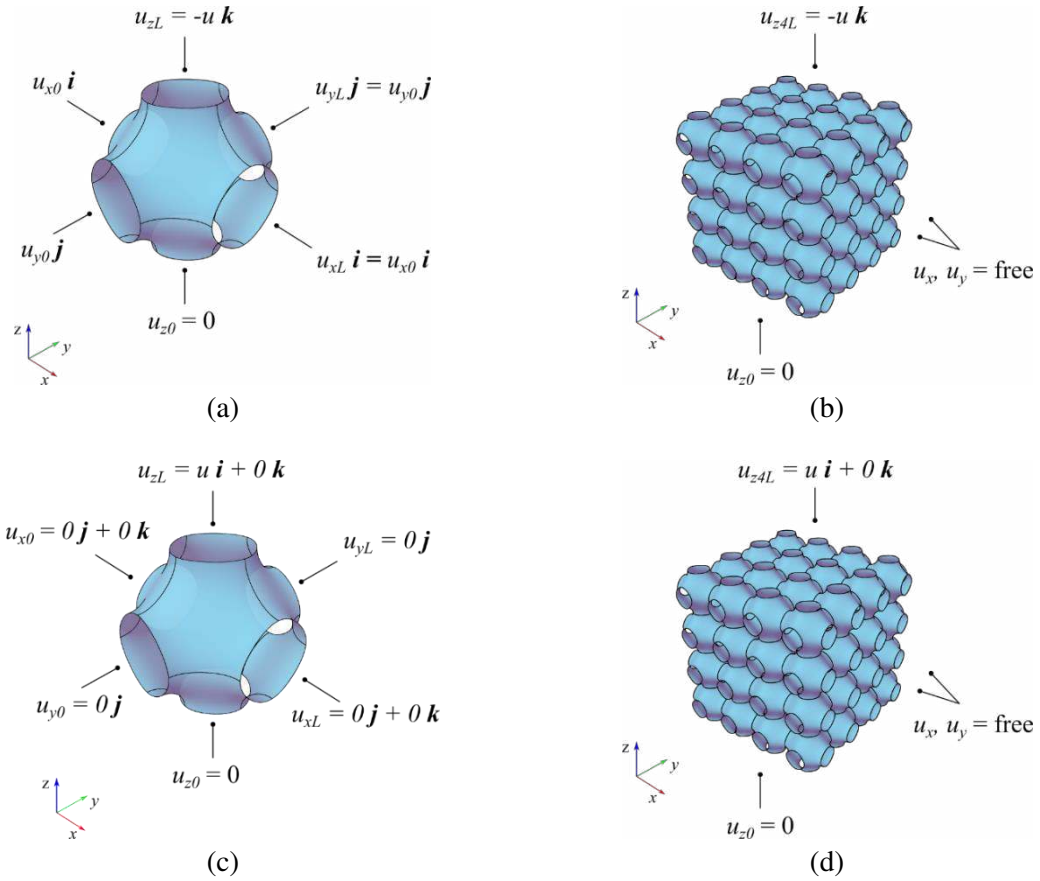

Fig. 3. Boundary conditions for Primitive TPMS FE simulation: periodic boundary conditions for a) uniaxial loading and c) simple shear on a single unit-cell; and mixed boundary conditions for b) compression and d) shear scenarios on matrix assemblies.

PBCs of translational symmetric unit-cells for uniaxial z displacement:

$$u_{x0} - u_{xL} = 0\,\boldsymbol{i}, \qquad u_{y0} - u_{yL} = 0\,\boldsymbol{j}, \qquad u_{z0} - u_{zL} = u\,\boldsymbol{k} \qquad \text{Eq. 3}$$

PBCs of translational symmetric unit-cells for shear loading:

$$u_{x0} = u_{xL} = 0\,\boldsymbol{j} + 0\,\boldsymbol{k}, \qquad u_{y0} = u_{yL} = 0\,\boldsymbol{j}, \qquad u_{z0} - u_{zL} = -u\,\boldsymbol{i} + 0\,\boldsymbol{k} \qquad \text{Eq. 4}$$

The pattern assembly case considers an arrangement of 64 unit-cells in a 4x4x4 distribution under mixed boundary conditions [21]. The testing size for assemblies was previously deemed acceptable for response prediction, due to their good compromise between convergence and computing times [30]–[32]. The employed boundary conditions are depicted on Fig. 3 for a Primitive unit-cell and a matrix assembly of patterns. The displacements at u_{z0} were constrained to prevent rigid body translations.

For the unit-cell scenarios, constraint equations were applied in opposite faces to guarantee the PBCs. FE simulation considered an isotropic material with an Elastic modulus E_0=200GPa, Shear modulus G_0=76.92GPa and a Poisson's ratio v_0=0.3. A displacement u with a magnitude of 0.01mm was applied on the top surface of the patterns, according to the defined boundary conditions, to account for elastic responses only. The reaction force F_R at the applied displacement and the von-Mises stress σ is obtained from the simulation results and employed in the posterior Equivalent material analysis.

2.3 Equivalent material methodology

The goal of the Equivalent material procedure is to obtain the relative Elastic modulus E^*, relative Shear modulus G^* and the relative Strength under compression σ^* and shear loads τ^* as a function of the relative density ρ^* of the pattern, according to a power-law defined by the Gibson-Ashby model [16]. For this, TPMS pattern's ρ^* is defined as the ratio between the volume of the pattern and the volume of the bounding box, as defined by Eq. 5.

$$\rho^* = \frac{v_{pattern}}{v_{bounding\ box}} \quad \text{Eq. 5}$$

Relative moduli, as defined by Eq. 6 and Eq. 7, corresponds to the ratio between the E or G of the pattern and the solid material E_0 or G_0 moduli, respectively. The relative Strength, is defined as the ratio between the strength of the pattern and the theoretical applied stress on the solid material, as shown on Eq. 8 and Eq. 9 for compression and shear loads, respectively.

$$E^* = \frac{E}{E_0} = c_1 {\rho^*}^{n_1} \quad \text{Eq. 6}$$

$$G^* = \frac{G}{E_0} = c_2 {\rho^*}^{n_2} \quad \text{Eq. 7}$$

$$\sigma^* = \frac{\sigma}{\sigma_0} = c_3 {\rho^*}^{n_3} \quad \text{Eq. 8}$$

$$\tau^* = \frac{\tau}{\sigma_0} = c_4 {\rho^*}^{n_4} \quad \text{Eq. 9}$$

The model's coefficient c is a constant of proportionality, which depends on the type of interconnectivity of the pattern. The exponent n is related to the mechanical response of the patterns [7]. From the Gibson-Ashby model, the relative modulus exponent n adopts a value of 1 and 2 for stretch-dominated and bending-dominated structures, respectively. Likewise, relative strength n coefficient is equal to 1 and 1.5 for stretch-dominated and bending-dominated structures. In general, structures with stretch-dominated deformation mechanism have a higher modulus and strength, while bending-dominated constructs have better energy absorption characteristics [33].

The pattern's E and G moduli can be found as the ratio between the applied stress (σ or τ) and the strain u/L. Similarly, σ and τ are related to the applied force over the area of the bounding box face related to the applied load. To determine the Gibson-Ashby model's coefficients, the results of the relative parameters are plotted with respect to different values of relative density ρ^*, and the data is approximated by non-linear regression methods to a power curve fit. Table 1 summarizes previous results found in the literature for sheet-based TPMS patterns.

In particular, the response of TPMS patterns geometries for relative elastic modulus and relative strength in compression can be employed to determine the required density of the equivalent cellular construct which would represent a solid material under the influence of a load compiling to a particular set of performance conditions, *i.e.* a permissible structure deformation u_{perm} and the employed material strength σ_{perm}. The values for total deformation u_{total} and maximum von Mises stress $\sigma_{von\ Mises}$ can be determined from a FEA of the solid material under the required loads. By combining Eq. 10 and Eq. 11 with Eq. 6 and Eq. 8, two density values can be determined. Ultimately, the solid material can be replaced by a TPMS construct designed to represent the bigger value of the two determined densities, thus obtaining a reduction on weight due to the pattern's geometric characteristics while maintaining the required design performance [25].

Table 1. Reported power-law model's coefficients by FE simulation and experimental testing.

Test conditions	ρ^* range	E^*		G^*		σ^*		τ^*		Study Ref.
		c_1	n_1	c_2	n_2	c_3	n_3	c_4	n_4	
FE simulation										
Primitive patterns										
Unit-cell	(0.02 – 0.20)	0.562	1.519	0.16	0.974	-	-	-	-	[19]
	(0.10 – 0.24)	0.61	1.57	0.16	0.97	0.794	1.36	0.256	0.98	[20]
Gyroid patterns										
Unit-cell	(0.02 – 0.20)	0.555	1.406	0.305	1.531	-	-	-	-	[19]
	(0.10 – 0.25)	0.51	1.38	-	-	0.44	1.24	-	-	[23]
Experimental testing										
Primitive patterns										
Cyl. Mtx. (Ti6Al4V)	(0.23 – 0.50)	0.107	1.12	-	-	0.967	1.77	-	-	[18]
4x4x4 (PA 2200)	(0.048 – 0.235)	0.395	1.518	-	-	1.104	1.749	-	-	[6]
6x6x6 (Maraging Stl.)	(0.073 – 0.206)	0.109	1.31	-	-	1.419	1.77	-	-	[22]
6x6x6 (Stainless Stl.)	(0.104 – 0.182)	0.56	1.89	-	-	2.67	2.23	-	-	[5]
Gyroid patterns										
Cyl. Mtx. (Ti6Al4V)	(0.31 – 0.49)	0.112	1.10	-	-	1.235	2.09	-	-	[18]
4x4x4 (PA 2200)	(0.07 – 0.46)	0.525	1.39	-	-	1.125	1.63	-	-	[17]
6x6x6 (Maraging Stl.)	(0.121 – 0.232)	0.103	1.23	-	-	0.885	1.43	-	-	[22]
6x6x6 (Stainless Stl.)	(0.141 – 0.244)	1.14	2.23	-	-	2.74	2.10	-	-	[5]

The absence of data is indicated by "-"
Test specimens as a cylindrical arrangement are denoted as "Cyl. Mtx."

$$E^* = \frac{u_{total}}{u_{perm}} \quad \text{Eq. 10} \qquad \sigma^* = \frac{\sigma_{von\ Mises}}{\sigma_{perm}} \quad \text{Eq. 11}$$

The values for total deformation u_{total} and maximum von Mises stress $\sigma_{von\ Mises}$ can be determined from a FEA of the solid material under the required loads. By combining Eq. 10 and Eq. 11 with Eq. 6 and Eq. 8, two density values can be determined. Ultimately, the solid material can be replaced by a TPMS construct designed to represent the bigger value of the two determined densities, thus obtaining a reduction on weight due to the pattern's geometric characteristics while maintaining the required design performance [25].

3 Results and Discussion

3.1 Uniaxial compression

Relative density of the tested patterns was determined from CAD data by using Eq. 5. The equations for Primitive are determined for a range on relative density between 0.094 and 0.473 (9.4% to 47.3%), and Gyroid models for a range between 0.124 and 0.624 (12.4% to 62.4%). FEA results for uniaxial compression are shown on Fig. 4 for Primitive and Gyroid patterns. Curves from FE results are depicted as a solid line, while results from experimental testing are depicted by dashed lines. Results from tests on unit-cells (UC) are represented by circular markers and results from matrix arrangements (Mtx) are marked by squares. The theoretical maximum coefficients from the Gibson-Ashby model are represented by dotted lines, corresponding to the curves for stretch and bending-dominated deformation mechanisms. The power-law model's coefficients from the fitted data are summarized on Table 2.

Table 2. Model's coefficients for uniaxial compression testing scenarios.

Test conditions	ρ^* range	E^*		σ^*	
		c_1	n_1	c_3	n_3
Primitive patterns					
Unit-cell	(0.094 – 0.471)	0.478	1.190	0.487	1.135
4x4x4 assembly	(0.095 – 0.473)	0.371	1.415	0.289	1.225
Ranges from literature	(0.02 – 0.50)	(0.107 – 0.61)	(1.12 – 1.89)	(0.794 – 2.67)	(1.36 – 2.23)
Gyroid patterns					
Unit-cell	(0.124 – 0.619)	0.413	1.351	0.432	1.679
4x4x4 assembly	(0.125 – 0.624)	0.402	1.176	0.426	1.537
Ranges from literature	(0.02 – 0.49)	(0.103 – 1.14)	(1.10 – 2.23)	(0.44 – 2.74)	(1.24 – 2.10)

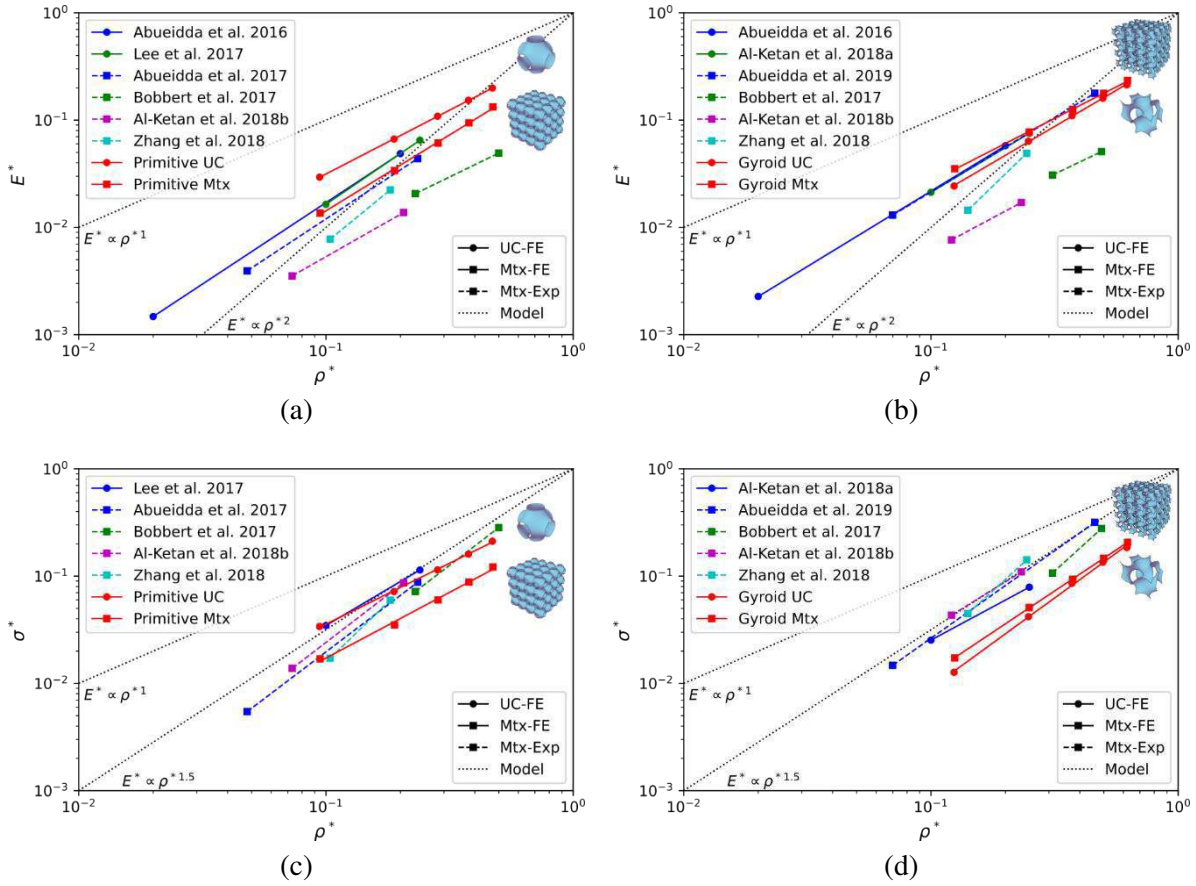

Fig. 4. Uniaxial compression results: Primitive a) Relative Elastic modulus and c) Relative Strength in compression; and Gyroid b) Relative Elastic modulus and d) Relative Strength in compression.

Is important to note that the relative elastic modulus on unit-cells was determined from the use of PBCs, in contrast with the employment of mixed boundary conditions found in some studies [20]. The latter approach establishes the periodic condition by assigning one side of the unit-cell interface with no displacement to simulate the contact with a neighbouring cell, while considering that the opposing face has no applied stresses, in addition to the load considerations. The employed PBCs on the current paper matches the deformation reaction in opposing sides of the unit-cell, thus adding an additional degree of constraint.

Overall results present a good agreement with the Gibson-Ashby model. As depicted by Fig. 4a for Primitive patterns, unit-cell results for E^* showed a stretch-dominated characteristic (n_1=1.190), while the 4x4x4 arrangement simulation evidenced a behaviour slightly leading to a bending-dominated mechanical response (n_1=1.415) similar to previous experimental results on matrix assemblies. In addition, σ^* responses, shown on Fig. 4c presents a stretch-dominated behaviour for both unit-cell (n_3=1.135) and the 4x4x4 assembly (n_3=1.225). Gyroid unit-cell and 4x4x4 matrix assembly results shows a stretch-dominated deformation behaviour for the relative elastic modulus (Fig. 4b, n_1=1.351 and n_1=1.176, respectively), while presenting a bending-dominating behaviour for relative strength in compression scenarios (Fig. 4d, n_3=1.679 and n_1=1.537 for UC and Mtx, respectively).

The comparison between the obtained FE simulation of 4x4x4 arrangements and unit-cell results are consistent with differences observed between experimental testing on patterns' assemblies and unit-cell FE simulation of past studies. For Primitive matrix assemblies, the value of c tends to be lower than the results obtained for unit-cells. In contrast, a good concordance between unit-cell simulation and matrix assemblies' compression experimental results have been previously established for Gyroid patterns, and was also found in the reported FEA results. As stated before, the c coefficient accounts for the interconnectivity of the patterns. The particular shape of Gyroid TPMS can potentially explain the better correlation between unit-cell and assemblies results, as the unit-cells have a higher degree of connections with neighbour cells, and, by extension, a better interaction of constraints when applying PBCs.

3.2 Shear loads

Primitive and Gyroid models were tested under shear loads following the boundary conditions defined on Fig. 3. FEA results are shown on Fig. 5 following the previously established results' representation convention. The summary for the determined model's coefficients can be consulted on Table 3.

Table 3. Model's coefficients for shear testing scenarios.

Test conditions	ρ^* range	G^*		τ^*	
		c_2	n_2	c_4	n_4
Primitive patterns					
Unit-cell	(0.094 – 0.471)	0.206	1.110	0.283	1.537
4x4x4 assembly	(0.095 – 0.473)	0.120	1.223	0.133	1.530
Ranges from literature	(0.02 – 0.24)	(0.16 – 0.16)	(0.97 – 0.974)	(0.256)	(0.98)
Gyroid patterns					
Unit-cell	(0.124 – 0.619)	0.195	1.237	0.239	1.277
4x4x4 assembly	(0.125 – 0.624)	0.118	1.213	0.161	1.193
Ranges from literature	(0.02 – 0.20)	(0.305)	(1.531)	-	-

The absence of data is indicated by "-"

Primitive patterns showed a stretch-dominated behaviour for relative shear modulus on both unit-cell (n_2=1.110) and matrix assembly (n_2=1.223) testing, as evidenced by Fig. 5a. Similarly, Gyroid pattern's results (Fig. 5b) showed stretch-dominated behaviour for unit-cells (n_2=1.237) and matrix (n_2=1.213). For relative strength under shear loads (Fig. 5c), Primitive unit-cell and matrix (n_4=1.537 and n_4=1.530, respectively) evidenced a bending-dominated deformation behaviour, indicating that Primitive TPMS deform under a combination of stretch and bending mechanisms under shear. In contrast, Gyroid unit-cell (n_4=1.277) and matrix (n_4=1.193) results indicate a stretch-dominated behaviour.

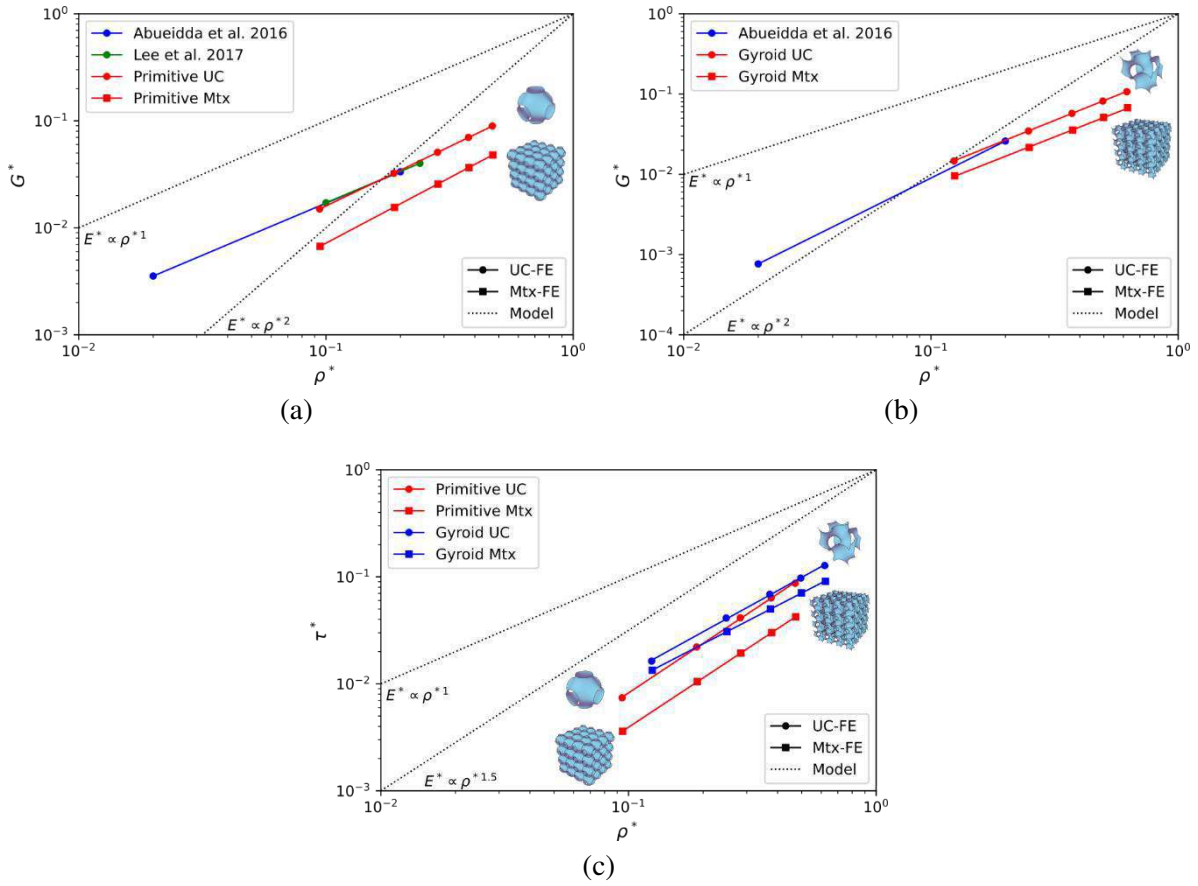

Fig. 5. Shear load results: Relative Shear modulus for a) Primitive and b) Gyroid patterns; and c) comparison of Relative Strength in shear for Primitive and Gyroid TPMS.

Similar to compression results, there is a difference in the c values obtained for Primitive and Gyroid patterns' unit-cells and matrix assemblies. However, there is no information available on the literature for this characteristic under shear loads to establish a comparison. For the reported results, all testing scenarios showed a decrease on c for matrix assemblies.

4 Conclusions

The mechanical response under compression and shear loads of Primitive and Gyroid TPMS was determined under a framework of equivalent material or metamaterial analysis. For compression scenarios, the relative elastic modulus and shear modulus of both Primitive and Gyroid pattern exhibited a stretch-dominated deformation behaviour, thus validating their employment on lightweight structural applications, where high stiffness and strength values are favoured over energy-absorption characteristics.

For Primitive patterns, unit-cell FE results estimate a higher resistance than the response obtained by the simulation of the matrix arrangement of patterns. In contrast, Gyroid results presents a better agreement between the two simulation scenarios. These effects are consistent to previous studies on FEA of unit-cells and experimental testing of patterns arrangements under compression loads. The same effect was found for the FE simulation of the patterns under shear loads, which has not been previously determined on the literature.

In the context of this study, a FGCM based on TPMS with variable density values can be developed, acting as an equivalent material which would replace an initial solid while simultaneously decreasing the weight and maintaining structural integrity. As FGCM are related to an ordered arrangement of cellular structures, model's results for relative elastic modulus and strength in compression from matrix assemblies' simulations are considered for the determination of local densities from deformation or stress mappings.

In summary, FEA of Primitive TPMS patterns arrangements exhibited a scaling by $\rho^{*1.415}$ for E^* and a scaling by $\rho^{*1.225}$ for σ^* a density range between 0.095 and 0.473, according to the Gibson-Ashby model for mechanic properties of cellular solids. Furthermore, matrix assemblies of Gyroid patterns showed a scaling by $\rho^{*1.176}$ for E^* and a scaling by $\rho^{*1.537}$ for σ^* for densities between 0.125 and 0.624. In general, Gyroid TPMS on a matrix arrangement exhibit a higher resistance than Primitive counterparts, evidenced by the results of the proportionality constant c for uniaxial compression and shear loads.

Acknowledgements

This work is supported by the ANR BeShape project, of the French Agence Nationale de la Recherche, Paris, France [grant number ANR-18-CE10-0014-01].

References

[1] M. K. Thompson *et al.*, 'Design for Additive Manufacturing: Trends, opportunities, considerations, and constraints', *CIRP Annals*, vol. 65, no. 2, pp. 737–760, Jan. 2016, doi: 10.1016/j.cirp.2016.05.004.
[2] M. F. Ashby and R. F. M. Medalist, 'The mechanical properties of cellular solids', *MTA*, vol. 14, no. 9, pp. 1755–1769, Sep. 1983, doi: 10.1007/BF02645546.
[3] I. Maskery, N. T. Aboulkhair, A. O. Aremu, C. J. Tuck, and I. A. Ashcroft, 'Compressive failure modes and energy absorption in additively manufactured double gyroid lattices', *Additive Manufacturing*, vol. 16, pp. 24–29, Aug. 2017, doi: 10.1016/j.addma.2017.04.003.
[4] R. Hedayati, A. M. Leeflang, and A. A. Zadpoor, 'Additively manufactured metallic pentamode meta-materials', *Appl. Phys. Lett.*, vol. 110, no. 9, p. 091905, Feb. 2017, doi: 10.1063/1.4977561.
[5] L. Zhang *et al.*, 'Energy absorption characteristics of metallic triply periodic minimal surface sheet structures under compressive loading', *Additive Manufacturing*, vol. 23, pp. 505–515, Oct. 2018, doi: 10.1016/j.addma.2018.08.007.
[6] D. W. Abueidda, M. Bakir, R. K. Abu Al-Rub, J. S. Bergström, N. A. Sobh, and I. Jasiuk, 'Mechanical properties of 3D printed polymeric cellular materials with triply periodic minimal surface architectures', *Materials & Design*, vol. 122, pp. 255–267, May 2017, doi: 10.1016/j.matdes.2017.03.018.
[7] D. Sharma and S. S. Hiremath, 'Additively manufactured mechanical metamaterials based on triply periodic minimal surfaces: Performance, challenges, and application', *Mechanics of Advanced Materials and Structures*, vol. 0, no. 0, pp. 1–31, Aug. 2021, doi: 10.1080/15376494.2021.1948151.
[8] H. Karcher, K. Polthier, J. Klinowski, and A. L. Mackay, 'Construction of triply periodic minimal surfaces', *Philosophical Transactions of the Royal Society of London. Series A: Mathematical, Physical and Engineering Sciences*, vol. 354, no. 1715, pp. 2077–2104, Sep. 1996, doi: 10.1098/rsta.1996.0093.
[9] A. L. Mackay, 'Periodic minimal surfaces', *Physica B+C*, vol. 131, no. 1–3, pp. 300–305, Aug. 1985, doi: 10.1016/0378-4363(85)90163-9.

[10] H. G. von Schnering and R. Nesper, 'Nodal surfaces of Fourier series: Fundamental invariants of structured matter', *Z. Physik B - Condensed Matter*, vol. 83, no. 3, pp. 407–412, Oct. 1991, doi: 10.1007/BF01313411.
[11] D. Li, W. Liao, N. Dai, and Y. M. Xie, 'Comparison of Mechanical Properties and Energy Absorption of Sheet-Based and Strut-Based Gyroid Cellular Structures with Graded Densities', *Materials*, vol. 12, no. 13, p. 2183, Jan. 2019, doi: 10.3390/ma12132183.
[12] R. Ambu and A. E. Morabito, 'Porous Scaffold Design Based on Minimal Surfaces: Development and Assessment of Variable Architectures', *Symmetry*, vol. 10, no. 9, Art. no. 9, Sep. 2018, doi: 10.3390/sym10090361.
[13] M. Zhao, D. Z. Zhang, F. Liu, Z. Li, Z. Ma, and Z. Ren, 'Mechanical and energy absorption characteristics of additively manufactured functionally graded sheet lattice structures with minimal surfaces', *International Journal of Mechanical Sciences*, vol. 167, p. 105262, Feb. 2020, doi: 10.1016/j.ijmecsci.2019.105262.
[14] M. F. Ashby, 'The properties of foams and lattices', *Philosophical Transactions of the Royal Society A: Mathematical, Physical and Engineering Sciences*, vol. 364, no. 1838, pp. 15–30, Jan. 2006, doi: 10.1098/rsta.2005.1678.
[15] R. Hedayati *et al.*, 'Isolated and modulated effects of topology and material type on the mechanical properties of additively manufactured porous biomaterials', *Journal of the Mechanical Behavior of Biomedical Materials*, vol. 79, pp. 254–263, Mar. 2018, doi: 10.1016/j.jmbbm.2017.12.029.
[16] L. J. Gibson and M. F. Ashby, *Cellular Solids: Structure and Properties*, 2nd ed. Cambridge: Cambridge University Press, 1997. doi: 10.1017/CBO9781139878326.
[17] D. W. Abueidda, M. Elhebeary, C.-S. (Andrew) Shiang, S. Pang, R. K. Abu Al-Rub, and I. M. Jasiuk, 'Mechanical properties of 3D printed polymeric Gyroid cellular structures: Experimental and finite element study', *Materials & Design*, vol. 165, p. 107597, Mar. 2019, doi: 10.1016/j.matdes.2019.107597.
[18] F. S. L. Bobbert *et al.*, 'Additively manufactured metallic porous biomaterials based on minimal surfaces: A unique combination of topological, mechanical, and mass transport properties', *Acta Biomaterialia*, vol. 53, pp. 572–584, Apr. 2017, doi: 10.1016/j.actbio.2017.02.024.
[19] D. W. Abueidda, R. K. Abu Al-Rub, A. S. Dalaq, D.-W. Lee, K. A. Khan, and I. Jasiuk, 'Effective conductivities and elastic moduli of novel foams with triply periodic minimal surfaces', *Mechanics of Materials*, vol. 95, pp. 102–115, Apr. 2016, doi: 10.1016/j.mechmat.2016.01.004.
[20] D.-W. Lee, K. A. Khan, and R. K. Abu Al-Rub, 'Stiffness and yield strength of architectured foams based on the Schwarz Primitive triply periodic minimal surface', *International Journal of Plasticity*, vol. 95, pp. 1–20, Aug. 2017, doi: 10.1016/j.ijplas.2017.03.005.
[21] H. Jia *et al.*, 'An experimental and numerical investigation of compressive response of designed Schwarz Primitive triply periodic minimal surface with non-uniform shell thickness', *Extreme Mechanics Letters*, vol. 37, p. 100671, May 2020, doi: 10.1016/j.eml.2020.100671.
[22] O. Al-Ketan, R. Rowshan, and R. K. Abu Al-Rub, 'Topology-mechanical property relationship of 3D printed strut, skeletal, and sheet based periodic metallic cellular materials', *Additive Manufacturing*, vol. 19, pp. 167–183, Jan. 2018, doi: 10.1016/j.addma.2017.12.006.
[23] O. Al-Ketan, R. Rezgui, R. Rowshan, H. Du, N. X. Fang, and R. K. A. Al-Rub, 'Microarchitected Stretching-Dominated Mechanical Metamaterials with Minimal Surface Topologies', *Advanced Engineering Materials*, vol. 20, no. 9, p. 1800029, 2018, doi: 10.1002/adem.201800029.
[24] E. A. Ramírez, N. Béraud, F. Pourroy, F. Villeneuve, and M. Museau, 'Design parameters effects on relative density of triply periodic minimal surfaces for additive manufacturing', *Procedia CIRP*, vol. 100, pp. 13–18, Jan. 2021, doi: 10.1016/j.procir.2021.05.002.

[25] A. H. Azman, 'Method for integration of lattice structures in design for additive manufacturing', PhD thesis, Université Grenoble Alpes, 2017. Accessed: Sep. 02, 2020. [Online]. Available: https://tel.archives-ouvertes.fr/tel-01688758
[26] E. A. Ramírez, N. Beraud, F. Pourroy, F. Villeneuve, and M. Museau, 'A design methodology for graded density triply periodic minimal surfaces', *Proceedings of the International Joint Conference on Mechanics, Design Engineering and Advanced Manufacturing (JCM 2022)*, 2022.
[27] A. Doi and A. Koide, 'An Efficient Method of Triangulating Equi-Valued Surfaces by Using Tetrahedral Cells', *IEICE TRANSACTIONS on Information and Systems*, vol. E74-D, no. 1, pp. 214–224, Jan. 1991.
[28] S. Li, 'Boundary conditions for unit cells from periodic microstructures and their implications', *Composites Science and Technology*, vol. 68, no. 9, pp. 1962–1974, Jul. 2008, doi: 10.1016/j.compscitech.2007.03.035.
[29] S. Li and A. Wongsto, 'Unit cells for micromechanical analyses of particle-reinforced composites', *Mechanics of Materials*, vol. 36, no. 7, pp. 543–572, Jul. 2004, doi: 10.1016/S0167-6636(03)00062-0.
[30] I. Maskery *et al.*, 'Insights into the mechanical properties of several triply periodic minimal surface lattice structures made by polymer additive manufacturing', *Polymer*, vol. 152, pp. 62–71, Sep. 2018, doi: 10.1016/j.polymer.2017.11.049.
[31] I. Maskery, A. O. Aremu, L. Parry, R. D. Wildman, C. J. Tuck, and I. A. Ashcroft, 'Effective design and simulation of surface-based lattice structures featuring volume fraction and cell type grading', *Materials & Design*, vol. 155, pp. 220–232, Oct. 2018, doi: 10.1016/j.matdes.2018.05.058.
[32] H. Yin, Z. Liu, J. Dai, G. Wen, and C. Zhang, 'Crushing behavior and optimization of sheet-based 3D periodic cellular structures', *Composites Part B: Engineering*, vol. 182, p. 107565, Feb. 2020, doi: 10.1016/j.compositesb.2019.107565.
[33] V. S. Deshpande, M. F. Ashby, and N. A. Fleck, 'Foam topology: bending versus stretching dominated architectures', *Acta Materialia*, vol. 49, no. 6, pp. 1035–1040, Apr. 2001, doi: 10.1016/S1359-6454(00)00379-7.